

2023 S.T. Yau High School Science Award

Research Report

The Team

Name of team member: Xi He
School: Northfield Mount Hermon
City, Country: Gill, United States

Name of supervising teacher: Yuanhao Li
Job Title: Postdoctoral research fellow
School/Institution: University of Pittsburgh
City, Country: Pittsburgh, United States

Title of Research Report

Alkylammonium Modified Photosensitizers Achieve Lysosome-Precision Photodynamic Therapy: Implications from Molecular Dynamics Simulations

Date

18/08/2023

Alkylammonium Modified Photosensitizers Achieve Lysosome-Precision Photodynamic Therapy: Implications from Molecular Dynamics Simulations

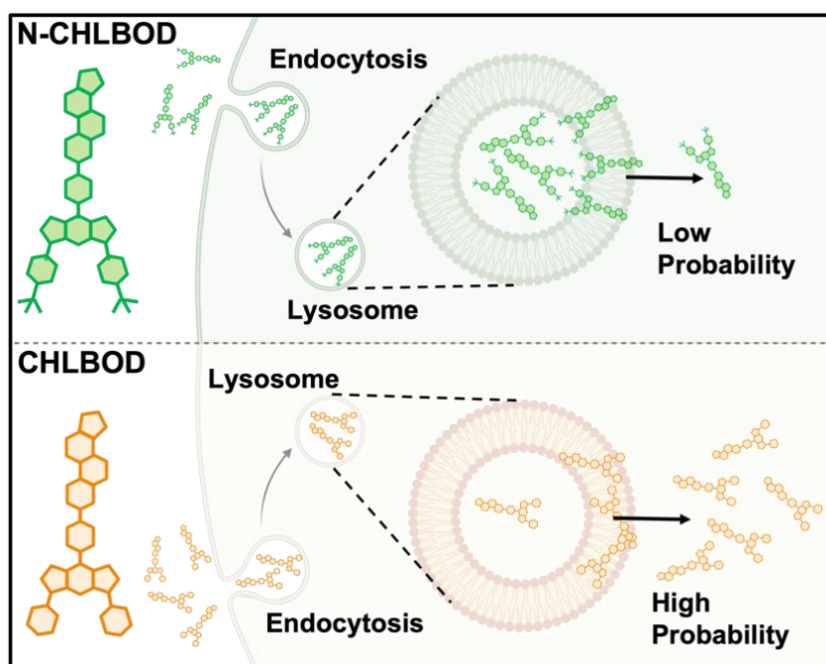
Xi He

Abstract

Photodynamic therapy (PDT) is one of the developing treatment modalities that has been clinically approved for cancer treatment. It uses an organic photosensitizer that harnesses the light energy and converts intracellular oxygens to reactive cytotoxic species. The resulting chemicals can then damage cells and lead to cancer cell death. However, the existing photosensitizers do not show cancer cell or organelle specificity, which lowers their treatment outcomes. In this project, we used molecular dynamic simulations to demonstrate that a straightforward alkylammonium modification on photosensitizers is able to endow conventional photosensitizers with the ability to target and accumulate in lysosomes. This acquired lysosome specificity may achieve the lysosome-precision PDT experimentally, which is expected to enhance the PDT outcomes. More importantly, such organelle-precision modifications have the potential to be extended beyond PDT treatment and make contribution to drug discovery and eventually cancer treatment.

Keywords: Cancer treatment, organelle-precision, photodynamic therapy, molecular dynamics simulations

Table of Content Graph



Declaration of Academic Integrity

The participating team declares that the paper submitted is comprised of original research and results obtained under the guidance of the instructor. To the team's best knowledge, the paper does not contain research results, published or not, from a person who is not a team member, except for the content listed in the references and the acknowledgment. If there is any misinformation, we are willing to take all the related responsibilities.

Names of team members Xi He

Signatures of team members 

Name of the instructor Yuanhao Li

Signature of the instructor 

Date 07/25/2023

Table of Contents

1 Introduction	1
2 Method	3
2.1 Photosensitizer Parameterization	3
2.2 Membrane Model Construction	4
2.3 Membrane Equilibration	5
2.4 Photosensitizer Partitioning into Membrane and Steered MD simulations	6
3 Results	6
3.1 Membrane Equilibration	6
3.2 Translocation of Photosensitizers into Membrane	7
3.3 Cross-membrane free energy profiles	9
4 Discussion	10
References	12
Acknowledgement	15

1 Introduction

Cancer is the second leading cause of death worldwide and remains a major threat to public health¹. Conventional therapies including surgery, radiotherapy, and chemotherapy have been playing an important role in cancer treatment^{2,3}. However, they demonstrate significant side effects, particularly the widespread damage to healthy cells⁴. To alleviate these side effects, new treatment modalities have been developed over the past decades. PDT is a minimally invasive safe therapy that focuses on local treatment with minimal side effects⁵. PDT includes 3 components : visible light, intracellular oxygen and photosensitizer. Common photosensitizers include porphyrin and its derivatives, phthalocyanine, BODIPY⁶. After accumulating photosensitizers in target cells, a specific wavelength is applied locally to activate the photosensitizer, which converts molecular oxygen to reactive oxygen species (ROS), causing damage to cancer cells (**Figure 1**). The generated ROS have a short life span (0.03–0.18 ms) and limited diffusion range (0.01–0.02 μm) in biological systems⁷. PDT, as a result, is usually limited by the spatiotemporal selectivity, and the subcellular location of the PSs may determine the therapeutic outcomes of PDT.

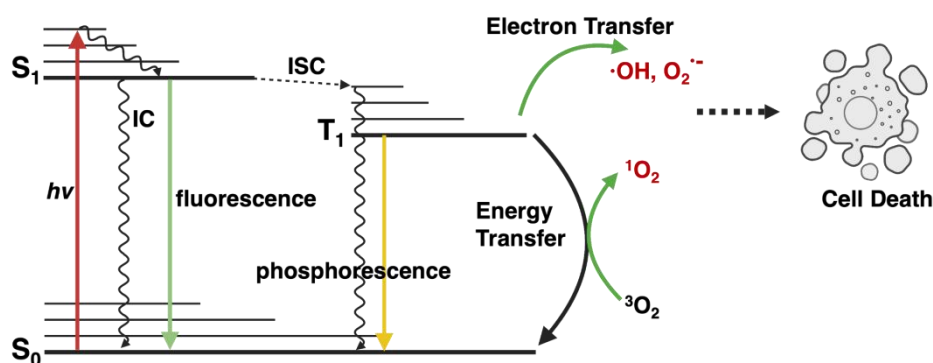


Figure 1. Mechanism of PDT treatment. After light irradiation, the ground state (S_0) photosensitizers would absorb the photo energy and be excited to S_1 state. During this state, it has chance to transfer to a triplet state (T_1), under which the photosensitizer may transfer energy to triplet oxygen (O_2^3) to singlet oxygen (O_2^1) or other reactive oxygen species to induce cell death.

Cellular organelles, such as endo/lysosome, endoplasmic reticulum, or mitochondrion, are cornerstones of cells and play vital roles in regulating and maintaining cell functions⁸. PDT damage to these organelles induces membrane permeabilization and expression of proapoptotic factors that subsequently initiate cell apoptosis. Thus, organelle precision theories are introduced for the sake of improved efficacy and reduced side effects. Previous organelle targeting strategies include mitochondrial targeting sequence, antibody-based targeting and peptide-based targeting⁹. With the

target modifications, treatment agents can then be brought approximal to the organelles and exert photo-damages, which would lead to more detrimental effects in cells as compared with random photo-damage¹⁰. In particular, lysosomes serve as the first machinery that processes exogenous materials or drugs after cellular internalization¹¹. The proteases and hydrolases in the lysosomes, once released to the cytosol by damage, could initiate cancer cell death. Therefore, targeting lysosomes have been now considered as a new and popular strategy to achieve organelle precision therapies.

The majority of existing photosensitizers do not possess targeting abilities to organelles. Studies have shown that amine drugs are more likely to accumulate in lysosomes as a result of protonation on the amine group¹². This phenomenon inspired us to use alkylammonium modification to improve the lysosome-targeting ability of photosensitizers. We hypothesize that such modification on photosensitizers will alter the kinetics and thermodynamics of the photosensitizers, which may allow the accumulation and prolong the retention of photosensitizers in the lysosomes during the treatment window. To study this, we seek to use molecular dynamics simulations as it could provide the thermodynamics and kinetic behaviors of the photosensitizers on the atomic level.

We designed two photosensitizers as shown in **Figure 2**. Both photosensitizers consisted of a cholesterol (CHL) moiety and a BODIPY (BOD) with biphenyl rings. The purpose of cholesterol moiety was to enhance the stability of photosensitizers in membrane structures while the BOD was the light sensitive part that can harvest the energy from irradiation to generate ROS. The only difference between the two photosensitizers was the tetramethyl ammonium modification on the biphenyl groups. The unmodified photosensitizer was termed as CHLBOD while the other one was N-CHLBOD. From MD simulations, we demonstrated that such simple modification was able to increase the retention of the N-CHLBOD in lysosomes and increase the energy barrier of crossing the lysosome membrane. Such chemical modifications are applicable in other areas such as small molecule drugs or biologics and drug design, which are important to further experimental tests.

2 Method

2.1 Photosensitizer Parameterization

To simulate the lipid bilayers, the SLipids force field is chosen as it is optimized and benchmarked for a number of lipids¹³. It is considered one of the best force field to represent lipids above their melting points. However, the force field does not include parameters for organic small molecules. Thus, we need to parameterize the photosensitizers separately. The general Amber force field (GAFF) was used for this purpose as it is commonly used to parameterize small organic molecules and has been tested as compatible to be compatible with SLipids force field^{14,15}.

We firstly used Chemdraw 16 to design the structures of two photosensitizers, the CHLBOD and N-CHLBOD (**Figure 2**). After cleaning up the structures, the simplified molecular-input line-entry system (SMILES), a string representation of molecules, was used to generate Gaussian input files with openbabel¹⁶. The structures of the photosensitizers were optimized by DFT calculations in Gaussian 16 using the B3LYP functional¹⁷. The Lanl2 basis set was used for iodine while 6-31G** was used for all other atoms¹⁸. The iodine atoms were treated with pseudopotential Lanl2 to facilitate the calculation. After optimization, the restricted electrostatic potential (RESP) charges were derived using the CHelpG library. The optimized structures were then converted to mol2 files using Gaussview, and the RESP charges were added manually. Initial topologies of PS were then generated by Acypype topology generator¹⁴. The additional nonbonded parameters and atom types from GAFF were added to the SLipids force field.

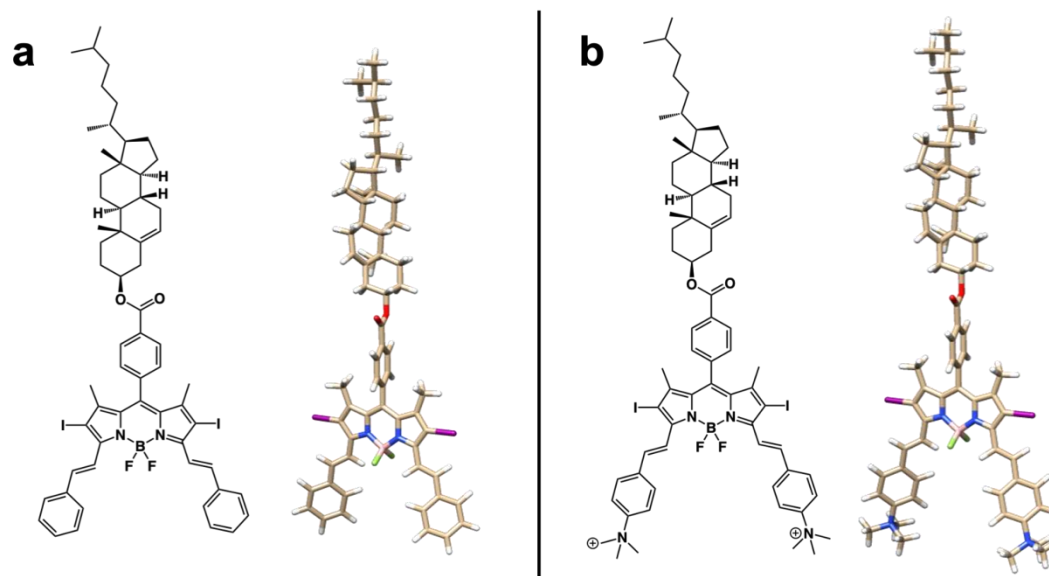


Figure 2. Initial chemical structures and DFT optimized topologies of (a) CHLBOD and (b) N-CHLBOD.

2.2 Membrane Model Construction

For the molecular dynamic simulations, a slice of lysosome phospholipid bilayer membrane was designed because simulating a whole lysosome would be intractable in all atom molecular dynamic simulations¹⁹. To mimic the behaviors of lysosomes, the 1,2-dimyristoyl-sn-glycero-3-phosphocholine (DMPC) lipid was chosen as it is the most abundant phospholipid. In addition, we added 38% cholesterol into the system to improve the stability and rigidity of the model²⁰. Since the cutoff for pairwise interactions is 12 Å, the box size was set to be larger than 24 Å to obey the minimum image convention. Additionally, to allow the photosensitizers to be in a non-interacting state, the water phase has to be thick enough for subsequent simulations. The thickness of the water layer on each side has to be at least 2.5 nm from the lipid head, which led to a length of 9.2 nm on the z axis. Thus, the simulated box was set to $4 \times 4 \times 9.2 \text{ nm}^3$. To calculate the numbers of each component, each lipid head was assumed as 0.65 nm^2 , which led to the estimation that for a plane of $4 \times 4 \text{ nm}^2$, 25 lipids were needed for each layer. Accordingly, 19 cholesterol molecules were added into the membrane. The composition of each component is shown in the table in **Figure 3**. Then, the lipid bilayer was constructed using packmol²¹. The lipids are properly oriented. After assembling the lipid bilayer with cholesterol, water molecules were added beyond the lipid bilayer to reach a

density of 1 g/cm^3 . The lysosomal membrane lipid bilayer model and its compositions are shown in **Figure 3** with periodic boundaries.

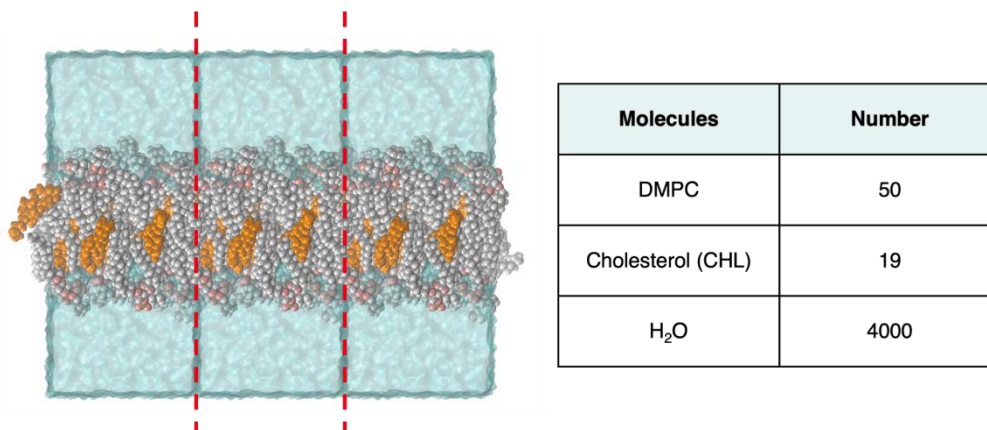


Figure 3. Snapshot and compositions of the lysosomal bilayer membrane model. The cholesterol is shown in orange and water is shown in cyan. The gray, pink, blue and white represent the carbon, oxygen, nitrogen and hydrogen atoms. The red dashed lines show the periodic boundaries of the simulation box.

2.3 Membrane Equilibration

Gromacs 2023.1 package was used to implement all molecular dynamics simulations²². TIP3P water model was used²³. Prior to equilibration, an energy minimization was conducted using the steepest descent algorithm to eliminate the unreasonable initial atom positions. All simulations were performed in NPT conditions with a constant pressure of 1 bar and a temperature of 310 K maintained by c-rescale²⁴ barostat and v-rescale²⁵ thermostat, respectively. The equilibration was completed after 25 ns with a time step of 1 fs. The output energies and trajectories were saved every 5 ps. The thermodynamic quantities including density, potential energy, and temperature were extracted from the trajectories to examine the equilibration. In addition, the density distribution of each component was plotted to show the symmetric structure of the equilibrated system. Snapshots of configurations were created by visual molecular dynamics (VMD) software²⁶.

2.4 Photosensitizer Partitioning into Membrane and Steered MD simulations

After equilibrating the membrane model, we then inserted each photosensitizer to the upper water phase to generate two model systems. The upper water phase was considered as the intra-lysosome compartment while the lower half as extra-lysosome compartment. To examine the partition of the photosensitizers into the membrane, we carried out long unbiased MD simulations until the photosensitizers stably translocated into the membrane. The z position and the partial densities of the photosensitizers were then extracted from the trajectories to examine the different location and orientation of the photosensitizers.

To mimic the cross-membrane behavior of each photosensitizer, using unbiased method would be intractable because it is impossible to sample the low-probability phase space. Thus, we performed steered MD simulations to allow the systems to sample the whole cross-membrane pathway. We used umbrella sampling to pull the photosensitizers out of the membrane with a harmonic potential of 500 kJ/mol/nm². The pulling rate was optimized to 0.001 nm/ps to maintain the equilibrium as much as possible. Sampling windows were selected by a distance interval of 0.25 nm along the Z axis to ensure the overlap of the phase space between each adjacent window²⁷. Each window was sampled for 30 ns and the last 10 ns were used for statistical analysis. The potential of mean force profiles was then calculated by the weighted histogram analysis method (wham) algorithm²⁸.

3 Results

3.1 Membrane Equilibration

Prior to modeling the photosensitizers, it is essential to obtain a uniform and well-equilibrated membrane structure. We first equilibrated the membrane with the NPT ensemble to produce reasonable bulk quantities. To check whether the membrane had been equilibrated, thermodynamic quantities including potential energy, density and temperature were extracted and plotted against simulation time. As shown in **Figure 4a-c**, potential energy, density and temperature had converged within the simulation period, indicating that the membrane had been equilibrated. In addition, we investigated the partial density of each component to ensure that the model was equilibrated on the atomic level. **Figure 4d** displays the distribution of

each component along the Z axis. The equilibrated structure is imposed for better visualization. By looking at the graph of partial density, we can see the partial overlapping of DMPC heads and water phase, indicating that the membrane was well solvated by the water. In addition, the cholesterol molecules were well-distributed inside DMPC layer. The overall density distribution of the model was symmetric in accordance with biological systems. Overall, the structure of the constructed membrane was reasonable and applicable to subsequent modeling and simulations.

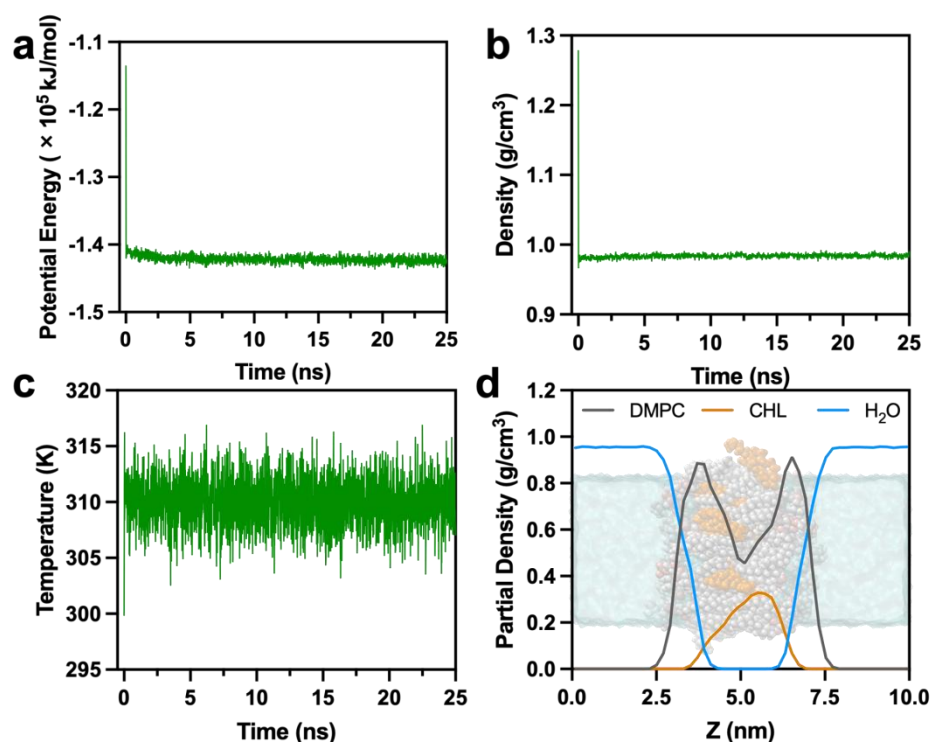


Figure 4. Equilibration of the lipid bilayer model. The convergence of the (a) potential energy, (b) density, and (c) temperature of the system. (d) The density plot of each component in the final 5 ns equilibration along the z coordinate.

3.2 Translocation of Photosensitizers into Membrane

We then inserted the two photosensitizers into the water phase respectively to generate two individual models, which were used to study the behavior of photosensitizers escaping the lysosomes. The photosensitizers' escaping the lysosomes was simplified as a two-step simulations. The first involved the free diffusion and partition of photosensitizers into the membrane and the second involved the cross-membrane behaviors. In this section, we discuss the varied kinetics of photosensitizers after alkylammonium modification.

The first metric we investigated was the simulation time taken for the photosensitizers to insert into the membrane. The distance between the photosensitizer and the center of the DMPC lipid layer was plotted against simulation time as shown in **Figure 5a**. A decrease of the Z distances indicated the insertion of photosensitizers into the membrane. The unmodified CHLBOD partitioned into the membrane in a short time around 45 ns. In contrast, the N-CHLBOD started to interact with the membrane after 150 ns. This implied that N-CHLBOD was more likely to retain in the lysosomes, while CHLBOD could easily translocate into membrane, after which the cross-membrane process may occur.

Furthermore, we investigated the partial density of the membrane after inserting CHLBOD and N-CHLBOD. It can be seen in **Figure 5b** that N-CHLBOD stayed closer to the surface of the DMPC membrane while CHLBOD was further inside the DMPC membrane. To verify this, we visualized configuration of each model as shown in **Figure 5c-d**.

Consistent with **Figure 5b**, N-CHLBOD showed a specific orientation with the positively-charged alkylammonium interacting with the negatively-charged phosphate group and water phase. However, CHLBOD fully partitioned into membrane. In conclusion, the unbiased simulation suggested that N-CHLBOD possessed longer lysosome time retention than CHLBOD. The oriented N-CHLBOD may also strongly interact with phospholipid head groups, which may slow down the photosensitizers crossing the lipid membrane.

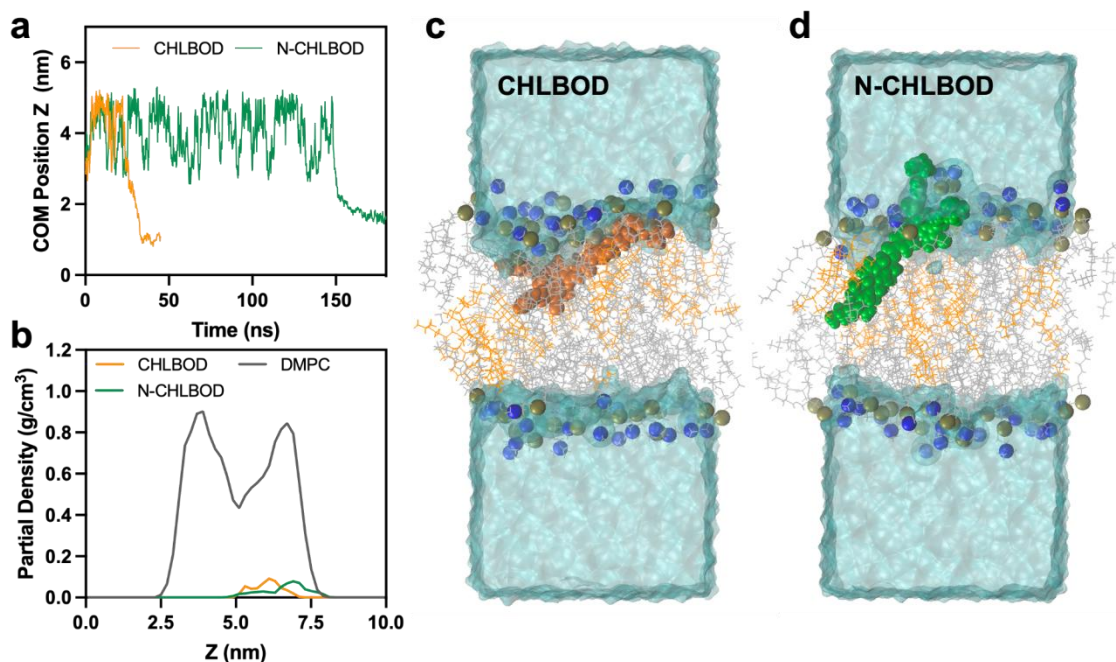


Figure 5. Photosensitizers partitioning into the bilayer membrane. (a) The center of mass position Z of photosensitizers relative to the center of box. (b) Partial density of each photosensitizer against the lipid DMPC along the z coordinate in the final 10 ns. Partitioned photosensitizers (c) CHLBOD and (d) N-CHLBOD in the membrane with different locations and orientations. The bulk water, the cholesterol and DMPC lipids are represented as cyan, orange and gray, respectively. The P and N atoms of the DMPC lipids head group are shown in blue and brown spheres. The photosensitizers are shown in the vdw model.

3.3 Cross-membrane free energy profiles

Based on this observation, we further hypothesized that the strong interaction between the alkylammonium group with the phospholipid head may also prevent N-CHLBOD diffusing out of lysosomes as more energy would be required to break the interactions. We then set out to simulate the cross-membrane process and calculate the corresponding free energy surface. For such a complicated system, unbiased MD will not be approachable within our computation capacity. Therefore, enhanced sampling was introduced to analyze the free energy when the photosensitizers crossed the membrane. In this case, we introduced a reaction coordinate Q (**Figure 6a**), which represented the diffusion progress across the membrane along the reaction pathway. Then we used umbrella sampling to compute the potential mean force (PME) profiles.

To calculate the PMF accurately, the phase space of selected adjacent windows along the coordinate Q should sufficiently overlap. This led to a total number of 24 and 25 windows for CHLBOD and N-CHLBOD, respectively. In **Figure 6b-c**, the histograms of each simulation window were plotted and showed reasonable counts and proper overlapping. Finally, in **Figure 6d**, it could be inferred that N-CHLBOD required significantly more energy (313 kJ/mol) than CHLBOD (137 kJ/mol) to move out of the membrane. This free energy difference roughly suggested that CHLBOD could diffuse out of the lysosome 4.54×10^{29} times faster than N-CHLBOD. All these results corroborated our hypothesis that N-CHLBOD would stay within the lysosomes for a longer time and cannot escape the membrane readily.

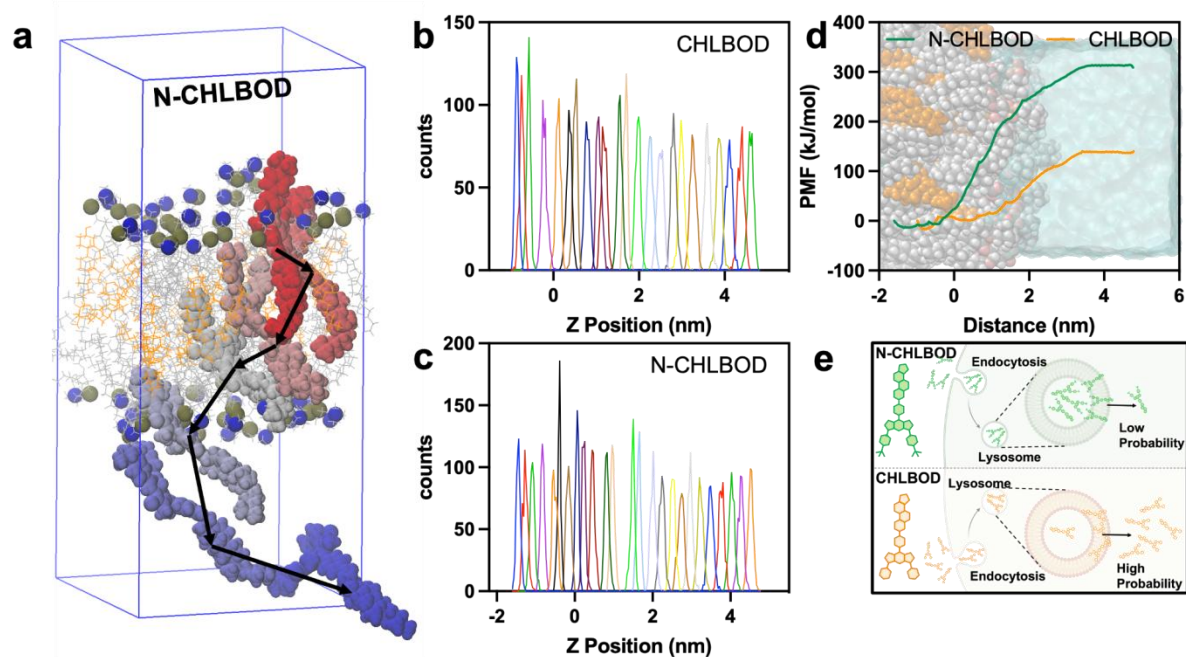


Figure 6. (a) Example on N-CHLBOD of the selected initial configurations from steered MD simulations. Only 6 snapshots were shown for clarity. The arrows indicate the pulling trajectories. In total, 25 windows were selected for N-CHLBOD and 24 for CHLBOD. The histogram of (b) CHLBOD and (c) N-CHLBOD shows the sufficient overlap of adjacent windows. (d) PMF profiles of CHLBOD and N-CHLBOD. (e) Schematic illustration of the probability of each photosensitizer's crossing the membrane.

4 Discussion

Designing agents that can target specific subcellular compartments, such as pivotal organelles, exhibits promise in cancer therapy^{10,29,30}. The agents could accumulate in target organelles and perturb their functions in a more intensive and detrimental manner. There are several advantages associated with such strategy. First, it can lower the dose of the anticancer agents and thus may reduce the side effects from the treatment. Secondly, as the agents can target and retain in the organelles, the treatment window can then be prolonged for better treatment schedule. In addition, such strategies can be readily coupled with other targeting techniques such as cancer cell specific targeting moieties³¹. This precision medicine strategy could further improve the anticancer efficacy.

In this project, we showcased that the simple and straightforward alkylammonium modification could endow the photosensitizers the ability to retain and accumulate in

lysosomes. The modeling and MD simulations have shown that the modified photosensitizer, N-CHLBOD, could be trapped in lysosomes. It also has a much higher free energy barrier than the unmodified photosensitizer CHLBOD to cross the lysosome membrane. As shown in **Figure 6e**, after cellular uptake of the photosensitizers, the N-CHLBOD has a lower probability to cross the lysosome membrane as compared with CHLBOD. These results indicate that the modified photosensitizers have the potential to achieve lysosome-precision PDT and eventually enhance the treatment outcomes.

In future studies, this mechanism of action from alkylammonium modification could be extended to other areas such as drug delivery and fluorescence imaging of lysosomes³². Although out of the scope of this project, experimental testing could be conducted to illustrate and confirm the expected results. It would be straightforward to use confocal imaging to show the colocalization of lysosomes with modified photosensitizers. In addition, one can use cell viability assays to compare the PDT efficacy of the two photosensitizers on cancer cells. In addition, this free energy calculation workflow is applicable in other organelle targeting systems. For instance, one use the umbrella sampling method to screen various small molecules that can target specific proteins on the organelle membranes. The candidates can thus be tested in experiments to examine their ability to carry cargos to the target organelles.

References

- 1 Siegel, R. L., Miller, K. D., Fuchs, H. E. & Jemal, A. Cancer statistics, 2022. *CA Cancer J Clin* **72**, 7-33, doi:10.3322/caac.21708 (2022).
- 2 Chandra, R. A., Keane, F. K., Voncken, F. E. M. & Thomas, C. R., Jr. Contemporary radiotherapy: present and future. *Lancet* **398**, 171-184, doi:10.1016/S0140-6736(21)00233-6 (2021).
- 3 Luo, D. *et al.* Pharmacokinetics and pharmacodynamics of liposomal chemophototherapy with short drug-light intervals. *J Control Release* **297**, 39-47, doi:<https://doi.org/10.1016/j.jconrel.2019.01.030> (2019).
- 4 Wang, K. & Tepper, J. E. Radiation therapy-associated toxicity: Etiology, management, and prevention. *CA Cancer J Clin* **71**, 437-454, doi:10.3322/caac.21689 (2021).
- 5 Gunaydin, G., Gedik, M. E. & Ayan, S. Photodynamic Therapy-Current Limitations and Novel Approaches. *Frontiers in Chemistry* **9**, doi:ARTN 69169710.3389/fchem.2021.691697 (2021).
- 6 Abrahamse, H. & Hamblin, M. R. New photosensitizers for photodynamic therapy. *Biochem J* **473**, 347-364, doi:10.1042/BJ20150942 (2016).
- 7 Niu, N. *et al.* A cell membrane-targeting AIE photosensitizer as a necroptosis inducer for boosting cancer theranostics. *Chem Sci* **13**, 5929-5937, doi:10.1039/d2sc01260j (2022).
- 8 Yang, J., Griffin, A., Qiang, Z. & Ren, J. Organelle-targeted therapies: a comprehensive review on system design for enabling precision oncology. *Signal Transduct Target Ther* **7**, 379, doi:10.1038/s41392-022-01243-0 (2022).
- 9 Saminathan, A., Zajac, M., Anees, P. & Krishnan, Y. Organelle-level precision with next-generation targeting technologies. *Nature Reviews Materials* **7**, 355-371, doi:10.1038/s41578-021-00396-8 (2022).
- 10 Wang, R., Li, X. & Yoon, J. Organelle-Targeted Photosensitizers for Precision Photodynamic Therapy. *ACS Appl Mater Interfaces* **13**, 19543-19571, doi:10.1021/acsami.1c02019 (2021).
- 11 Qiu, J. & Xia, Y. Killing cancer cells by rupturing their lysosomes. *Nat Nanotechnol* **15**, 252-253, doi:10.1038/s41565-020-0639-z (2020).
- 12 Kaufmann, A. M. & Krise, J. P. Lysosomal sequestration of amine-containing drugs: analysis and therapeutic implications. *J Pharm Sci* **96**, 729-746, doi:10.1002/jps.20792 (2007).

- 13 Grote, F. & Lyubartsev, A. P. Optimization of Slipids Force Field Parameters Describing Headgroups of Phospholipids. *J Phys Chem B* **124**, 8784-8793, doi:10.1021/acs.jpcc.0c06386 (2020).
- 14 Wang, J., Wang, W., Kollman, P. A. & Case, D. A. Automatic atom type and bond type perception in molecular mechanical calculations. *Journal of Molecular Graphics and Modelling* **25**, 247-260, doi:<https://doi.org/10.1016/j.jmgm.2005.12.005> (2006).
- 15 Wang, J., Wolf, R. M., Caldwell, J. W., Kollman, P. A. & Case, D. A. Development and testing of a general amber force field. *J Comput Chem* **25**, 1157-1174, doi:10.1002/jcc.20035 (2004).
- 16 Hirohara, M., Saito, Y., Koda, Y., Sato, K. & Sakakibara, Y. Convolutional neural network based on SMILES representation of compounds for detecting chemical motif. *BMC Bioinformatics* **19**, 526, doi:10.1186/s12859-018-2523-5 (2018).
- 17 Gaussian 16 Rev. C.01 (Wallingford, CT, 2016).
- 18 Yang, Y., Weaver, M. N. & Merz, K. M., Jr. Assessment of the “6-31+G** + LANL2DZ” Mixed Basis Set Coupled with Density Functional Theory Methods and the Effective Core Potential: Prediction of Heats of Formation and Ionization Potentials for First-Row-Transition-Metal Complexes. *The Journal of Physical Chemistry A* **113**, 9843-9851, doi:10.1021/jp807643p (2009).
- 19 Sobot, D. *et al.* Conjugation of squalene to gemcitabine as unique approach exploiting endogenous lipoproteins for drug delivery. *Nature Communications* **8**, 15678, doi:10.1038/ncomms15678 (2017).
- 20 Trivedi, P. C., Bartlett, J. J. & Pulinilkunnil, T. Lysosomal Biology and Function: Modern View of Cellular Debris Bin. *Cells* **9**, doi:10.3390/cells9051131 (2020).
- 21 Martinez, L., Andrade, R., Birgin, E. G. & Martinez, J. M. PACKMOL: a package for building initial configurations for molecular dynamics simulations. *J Comput Chem* **30**, 2157-2164, doi:10.1002/jcc.21224 (2009).
- 22 Abraham, M. J. *et al.* GROMACS: High performance molecular simulations through multi-level parallelism from laptops to supercomputers. *SoftwareX* **1-2**, 19-25, doi:<https://doi.org/10.1016/j.softx.2015.06.001> (2015).
- 23 Harrach, M. F. & Drossel, B. Structure and dynamics of TIP3P, TIP4P, and TIP5P water near smooth and atomistic walls of different hydroaffinity. *J Chem Phys* **140**, 174501, doi:10.1063/1.4872239 (2014).
- 24 Bernetti, M. & Bussi, G. Pressure control using stochastic cell rescaling. *J Chem Phys* **153**, 114107, doi:10.1063/5.0020514 (2020).
- 25 Bussi, G., Donadio, D. & Parrinello, M. Canonical sampling through velocity rescaling. *The Journal of Chemical Physics* **126**, doi:10.1063/1.2408420 (2007).

- 26 Humphrey, W., Dalke, A. & Schulten, K. VMD: visual molecular dynamics. *J Mol Graph* **14**, 33-38, 27-38, doi:10.1016/0263-7855(96)00018-5 (1996).
- 27 You, W., Tang, Z. & Chang, C.-e. A. Potential Mean Force from Umbrella Sampling Simulations: What Can We Learn and What Is Missed? *Journal of Chemical Theory and Computation* **15**, 2433-2443, doi:10.1021/acs.jctc.8b01142 (2019).
- 28 Hub, J. S., de Groot, B. L. & van der Spoel, D. g_wham—A Free Weighted Histogram Analysis Implementation Including Robust Error and Autocorrelation Estimates. *Journal of Chemical Theory and Computation* **6**, 3713-3720, doi:10.1021/ct100494z (2010).
- 29 Iulianna, T., Kuldeep, N. & Eric, F. The Achilles' heel of cancer: targeting tumors via lysosome-induced immunogenic cell death. *Cell Death & Disease* **13**, 509, doi:10.1038/s41419-022-04912-8 (2022).
- 30 Ubah, O. C. & Wallace, H. M. Cancer therapy: Targeting mitochondria and other sub-cellular organelles. *Curr Pharm Des* **20**, 201-222, doi:10.2174/13816128113199990031 (2014).
- 31 Li, Z., Zou, J. & Chen, X. In Response to Precision Medicine: Current Subcellular Targeting Strategies for Cancer Therapy. *Adv Mater* **35**, e2209529, doi:10.1002/adma.202209529 (2023).
- 32 Choi, N. E., Lee, J. Y., Park, E. C., Lee, J. H. & Lee, J. Recent Advances in Organelle-Targeted Fluorescent Probes. *Molecules* **26**, doi:10.3390/molecules26010217 (2021).

Acknowledgement

I would like to express my sincere gratitude to Dr. Yuanhao Li for his useful guidance and discussions throughout this research. His expertise in computational chemistry has been instrumental in assisting me to complete the MD simulations.